Chalcogenide Letters Vol. 22, No. 8, August 2025, p. 693 - 705

Design and synthesis of diketopyrrolopyrrole-CdS hybrid nanostructures for enhanced photovoltaic applications

Q. Fei *, B. Jin, B. C. Jiang, J. S. Huang, L. Li
School of Mechanical and Electrical Engineering, Guangdong University of Science and Technology, Dongguan, 523083, China

An innovative hybrid nanostructure composed of diketopyrrolopyrrole (DPP) oligomers and cadmium sulfide (CdS) nanoparticles was developed to enhance the efficiency of organic–inorganic photovoltaic devices. The DPP-CdS hybrids were synthesized via a solution-phase mixing method, resulting in uniform nanoparticle dispersion along polymer fibrils and strong interfacial coupling. Structural characterization confirmed the coexistence of crystalline CdS domains and partially ordered DPP phases, while spectroscopic analyses indicated notable redshifts and band broadening, evidencing electronic interactions at the interface. The hybrid material displayed significantly broadened light absorption across the 400–700 nm range and an optimized optical bandgap of ~1.92 eV. When implemented in inverted bulk heterojunction solar cells (ITO/PEDOT:PSS/DPP-CdS/$PC_{71}BM$/Al), the active layer enabled a short-circuit current density of 11.3 mA/cm², open-circuit voltage of 0.82 V, and a power conversion efficiency (PCE) of 5.93%—more than double the PCEs of devices with only DPP (2.61%) or CdS (1.35%). External quantum efficiency exceeded 60% at peak wavelengths, confirming efficient exciton generation and charge extraction. Furthermore, electrochemical impedance spectroscopy showed a reduced charge transfer resistance of 238 Ω, while transient photovoltage measurements revealed an extended carrier lifetime of 6.10 μs, indicating minimized recombination losses. These improvements are attributed to favorable energy level alignment, enhanced morphology, and interfacial engineering in the DPP-CdS hybrids. This work demonstrates the potential of combining conjugated organics with tailored inorganic nanostructures to overcome current performance limitations in hybrid photovoltaics and provides a scalable strategy for next-generation solar energy materials.

(Received April 15, 2025; Accepted August 7, 2025)

Keywords: Charge recombination, Nanocomposites, Optical absorption, Interface engineering, Carrier dynamics

* Corresponding author: m13262572178_1@163.com
https://doi.org/10.15251/CL.2025.228.693

1. Introduction

The accelerating global demand for sustainable and renewable energy has intensified the development of next-generation photovoltaic (PV) technologies. Among various options, solar energy stands as a virtually inexhaustible resource, and its direct conversion into electricity using solar cells continues to be a focal point of both academic and industrial research [1]. Traditional silicon-based photovoltaics, though dominating the commercial landscape, are approaching their theoretical efficiency limits and are constrained by issues such as high manufacturing costs, rigid structures, and energy-intensive production processes [2,3]. These limitations have stimulated a paradigm shift toward solution-processable, low-cost, and flexible alternatives—particularly organic and hybrid organic–inorganic solar cells [4]. Hybrid photovoltaics, which marry the tunable optoelectronic properties of organic semiconductors with the robust charge-transport capabilities of inorganic nanomaterials, present a promising pathway to overcome current efficiency bottlenecks [5]. Within this context, diketopyrrolopyrrole (DPP)-based polymers and small molecules have garnered considerable attention due to their outstanding π-conjugation, thermal stability, and versatile functionalization capabilities [6]. Their ability to serve as both donors and acceptors in bulk heterojunction solar cells has been explored extensively, and more recently, efforts have been directed toward integrating DPP units into hybrid architectures.

On the inorganic front, cadmium sulfide (CdS) has long been utilized in optoelectronics due to its suitable bandgap (~2.4 eV), high electron mobility, and stability under ambient conditions [7]. It is widely adopted as a buffer or window layer in thin-film solar cells, and its capability to transport electrons efficiently while acting as a hole-blocking layer renders it a valuable component in hybrid junctions. However, CdS suffers from weak absorption in the longer-wavelength range and relatively low exciton dissociation when used alone [8]. Thus, combining it with a strong light-harvesting and hole-conducting material, such as a DPP-based semiconductor, could create a synergistic interface that enhances photon harvesting, exciton dissociation, and charge separation.

Device efficiency in hybrid systems is largely governed by the interfacial characteristics at the heterojunction, which dictate charge transport and separation. Effective charge transfer and minimal recombination losses require a well-matched energy level alignment between the donor and acceptor, as well as intimate physical contact to facilitate exciton diffusion within the limited diffusion length of organic semiconductors [9]. DPP molecules offer the flexibility to fine-tune their frontier molecular orbitals through side-chain engineering, allowing their HOMO and LUMO levels to be closely aligned with those of common inorganic semiconductors like CdS. This electronic compatibility opens up the potential for constructing favorable type-II heterojunctions, in which electrons transfer from the organic donor to the inorganic acceptor, while holes remain in the DPP phase.

Beyond energetics, the morphology of the hybrid interface is another critical factor. CdS nanostructures can be synthesized with controlled size, crystallinity, and dimensionality—ranging from quantum dots to nanorods to nanosheets—thus providing a modular platform for interfacial engineering [10,11]. These nanostructures offer high surface-to-volume ratios and can serve as scaffolds for DPP molecules to anchor, enabling a more interconnected charge transport network. By optimizing synthesis parameters such as precursor concentration, temperature, and reaction time, it is possible to control the spatial distribution and interfacial intimacy of DPP and CdS, further influencing the charge separation efficiency [12]. Despite these promising attributes, few studies

have systematically explored DPP-CdS hybrid systems for photovoltaic applications, particularly in terms of correlating their synthesis pathways, interfacial structure, and optoelectronic performance. This gap in the literature presents an opportunity to investigate how rational design of DPP-CdS nanocomposites can lead to efficient light-harvesting assemblies. In our work, we propose a novel class of hybrid nanostructures composed of diketopyrrolopyrrole derivatives and cadmium sulfide nanoparticles, prepared via a solution-phase synthetic route that ensures uniform dispersion and optimal interface formation.

We aim to address several key challenges in hybrid solar cell design. First, we focus on achieving broadband absorption by leveraging the complementary absorption spectra of DPP and CdS. Second, we emphasize the formation of a well-aligned heterojunction with minimized interfacial defects, to reduce recombination losses and facilitate rapid charge extraction. Third, we investigate how morphological and structural features—such as particle size, crystallinity, and distribution—affect the overall photovoltaic response. To this end, we fabricate and characterize a series of DPP-CdS nanocomposites. We also fabricate photovoltaic devices employing these hybrid materials as the active layer, configured in an inverted bulk heterojunction architecture, and evaluate their performance under standard illumination conditions. Emphasis is placed on understanding how variations in synthesis parameters (e.g., DPP:CdS ratio, annealing temperature) influence material properties and device efficiency.

2. Materials and methods

2.1. Chemicals and materials

The diketopyrrolopyrrole (DPP) monomer was synthesized in-house based on a two-step Knoevenagel condensation and subsequent Suzuki cross-coupling strategy. Starting materials including 3,6-bis(5-bromothiophen-2-yl)-2,5-dihydropyrrolo[3,4-c]pyrrole-1,4-dione and 2,5-bis(trimethylstannyl)thiophene were purchased from Shanghai Aladdin Biochemical Technology Co., Ltd. N-bromosuccinimide (NBS), 1,2-dichlorobenzene, potassium carbonate, and $Pd(PPh_3)_4$ catalyst were obtained from Chengdu Kelong Chemical Reagents Co., Ltd. Cadmium nitrate tetrahydrate, thiourea, and ammonia solution were purchased from Sinopharm Chemical Reagent Co., Ltd. These were used for the aqueous-phase synthesis of CdS nanoparticles. Poly(3,4-ethylenedioxythiophene):poly(styrenesulfonate) (PEDOT:PSS, Clevios P VP AI 4083) was acquired from Heraeus China. $PC_{71}BM$ and anhydrous chlorobenzene were obtained from Xi'an Polymer Light Technology Corp. Transparent ITO-coated glass substrates were sourced from Zhuhai Kaivo Optoelectronic Technology Co., Ltd., while high-purity aluminum wire for cathode deposition was supplied by Beijing LT Scientific Instrument Co., Ltd.

2.2. Synthesis of DPP-CdS Hybrid Nanostructures

Briefly, 1.0 mmol of 3,6-bis(5-bromothiophen-2-yl)-DPP and 1.2 mmol of 2,5-bis(trimethylstannyl)thiophene were dissolved in 25 mL of anhydrous toluene. To this solution, 0.05 mmol of $Pd(PPh_3)_4$ was added, and the reaction was stirred at 110 °C for 24 h. Upon completion, the crude product was purified by silica column chromatography using hexane:chloroform (2:1 v/v) as eluent to yield the desired DPP oligomer.

Cadmium sulfide nanoparticles were synthesized via a simple aqueous co-precipitation method. In a typical procedure, 10 mmol of $Cd(NO_3)_2 \cdot 4H_2O$ was dissolved in 50 mL of water. Separately, 10 mmol of thiourea was dissolved in 50 mL of aqueous ammonia (pH adjusted to ~10.5). The thiourea solution was added dropwise to the cadmium nitrate solution under constant stirring at 60 °C. The reaction mixture was maintained at this temperature for 2 h, during which CdS precipitated gradually.

To fabricate the DPP-CdS hybrid nanostructure, a post-synthetic mixing approach was adopted. Equal masses of purified DPP oligomer and CdS nanoparticles were dispersed in 10 mL of chlorobenzene containing 5% v/v 1,8-diiodooctane (DIO) as a processing additive. The mixture was subjected to mild bath sonication for 1 h to ensure uniform dispersion and promote non-covalent interactions at the interface. The resulting suspension was further stirred for 12 h to allow for sufficient interaction between the organic and inorganic phases.

2.3. Device fabrication

Photovoltaic devices were constructed using an inverted architecture with the layer sequence: ITO/PEDOT:PSS/DPP-CdS/$PC_{71}BM$/Al. Glass substrates coated with ITO were subjected to successive ultrasonic cleaning steps in acetone, isopropanol, and deionized water, each for 15 minutes. This was followed by ultraviolet-ozone surface treatment for 20 minutes to enhance wettability and remove residual contaminants. A thin PEDOT:PSS film (~35 nm) was deposited onto the cleaned substrates via spin-coating at 4000 rpm for 60 seconds, then thermally treated at 150 °C for 15 minutes in ambient conditions to form the hole-transport layer.

After cooling, the substrates were transferred into a nitrogen-filled glovebox. The active layer was deposited by spin-coating a DPP-CdS hybrid dispersion onto the PEDOT:PSS film at 1500 rpm for 30 seconds, resulting in an approximate thickness of 100 nm. The coated films were subsequently annealed at 120 °C for 10 minutes to enhance crystallinity and improve interfacial compatibility. Next, a solution of $PC_{71}BM$ (20 mg/mL in chlorobenzene) was applied over the hybrid layer via spin-coating at 2000 rpm for 45 seconds. Finally, an aluminum electrode (approximately 80 nm thick) was deposited through thermal evaporation under high vacuum, with the effective device area defined as 0.1 cm^2.

3. Results and discussion

3.1. Morphological and structural characterization

Understanding the morphology and crystalline structure of the active materials is essential for correlating material properties with device performance. In this section, we analyze the structural features of pristine CdS nanoparticles, pure DPP oligomer, and their hybrid DPP-CdS nanocomposites through a combination of electron microscopy, diffraction, vibrational spectroscopy, and optical measurements. Figure 1 presents SEM and TEM images that reveal the morphological evolution upon hybrid formation. The SEM micrograph of CdS nanoparticles (Figure 1a) shows a dense aggregation of nearly spherical particles with diameters ranging from 20 to 40 nm. These particles display moderate surface roughness, indicating partial coalescence during precipitation [13]. In contrast, the SEM image of the pure DPP film (Figure 1b) demonstrates a typical fibrillar network with an interlaced morphology, characteristic of π-conjugated polymers with strong

interchain stacking. These fibrils are approximately 80–120 nm in diameter and several micrometers in length, consistent with extended chain alignment in spin-coated films. TEM imaging of the DPP-CdS hybrid nanostructures (Figure 1c) reveals a uniform distribution of CdS nanoparticles embedded within the DPP matrix. The nanoparticles appear well-dispersed along the polymeric fibrils, forming continuous conduction pathways [14].

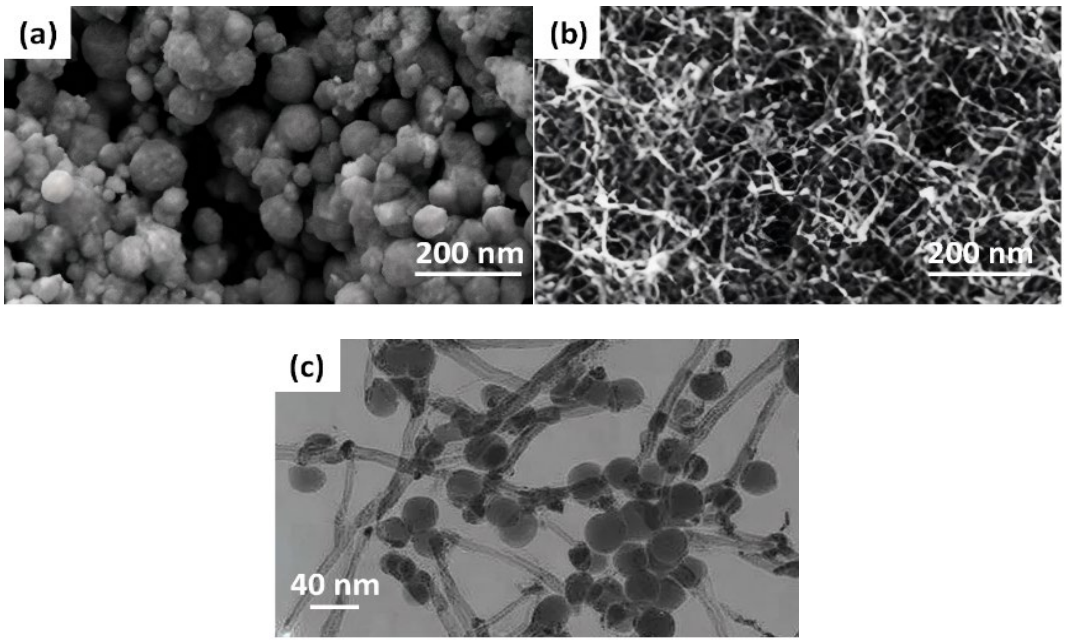

Fig. 1. (a) SEM of CdS nanoparticles showing spherical aggregates; (b) SEM of DPP film displaying fibrillar morphology; (c) TEM of DPP-CdS showing homogeneous nanoparticle dispersion.

To investigate crystallinity and phase composition, XRD measurements were conducted on all samples (Figure 2). The XRD pattern of CdS shows distinct diffraction peaks at $2\theta = 26.5°$, 43.8°, and 51.9°, which can be indexed to the (002), (110), and (112) planes of hexagonal wurtzite CdS, indicating good crystallinity [15]. In contrast, the DPP sample exhibits a broad hump centered at around 21°, characteristic of the π–π stacking distance in the disordered conjugated polymer. The DPP-CdS hybrid displays both the CdS crystalline peaks and a reduced polymer halo, suggesting the coexistence of crystalline inorganic and partially ordered organic domains [15]. The relative intensity of CdS peaks in the hybrid is slightly suppressed compared to pristine CdS, possibly due to the encapsulating polymer matrix limiting long-range ordering.

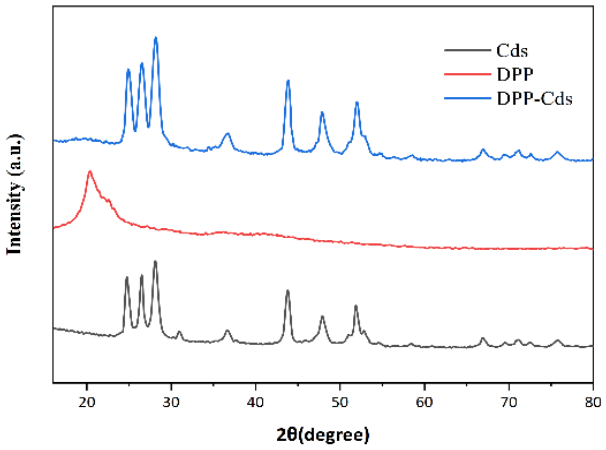

Fig. 2. XRD patterns of CdS, DPP, and DPP-CdS hybrid materials.

Chemical bonding and interaction between CdS and DPP components were analyzed via FTIR and Raman spectroscopy (Figure 3). The FTIR spectrum of DPP exhibits prominent peaks at 1690 cm^{-1} (C=O stretching of the diketopyrrolopyrrole core), 1525 cm^{-1} (C=C stretching in thiophene), and 1290 cm^{-1} (C–N stretching), while the CdS spectrum displays weak vibrational features due to the ionic nature of the compound. In the DPP-CdS hybrid, a noticeable red shift of the C=O stretching to 1678 cm^{-1} and broadening of the C–N stretching mode suggest hydrogen bonding or dipole interactions at the interface [16]. Raman spectra further support this, where the characteristic CdS longitudinal optical (LO) phonon peak at 303 cm^{-1} is retained but exhibits slight broadening and downshift in the hybrid, indicative of phonon confinement and surface interaction with the polymer chains [17].

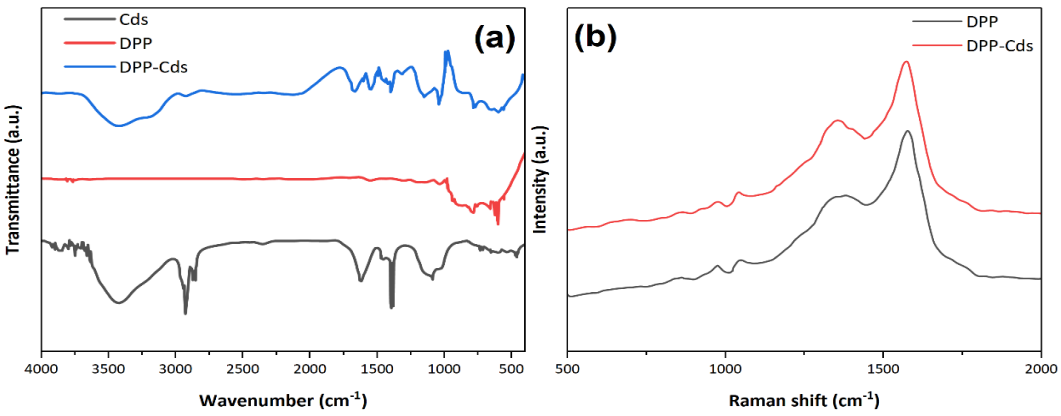

Fig. 3. (a) FTIR of pure DPP, CdS, and DPP-CdS hybrid. (b) Raman spectra of pure DPP and DPP-CdS hybrid.

Optical absorption properties of the samples were evaluated using UV-Vis spectroscopy, as shown in Figure 4. The CdS nanoparticles exhibit a strong absorption edge near 520 nm, corresponding to a bandgap of ~2.38 eV, as calculated from the Tauc plot (inset). Notably, the DPP-CdS hybrid demonstrates enhanced absorbance across the 400–700 nm region, with a slightly red-shifted shoulder, suggesting strong electronic coupling or Förster-type energy transfer between the two components [16]. The calculated optical bandgap of the hybrid is ~1.92 eV, indicating improved light-harvesting capability due to extended absorption.

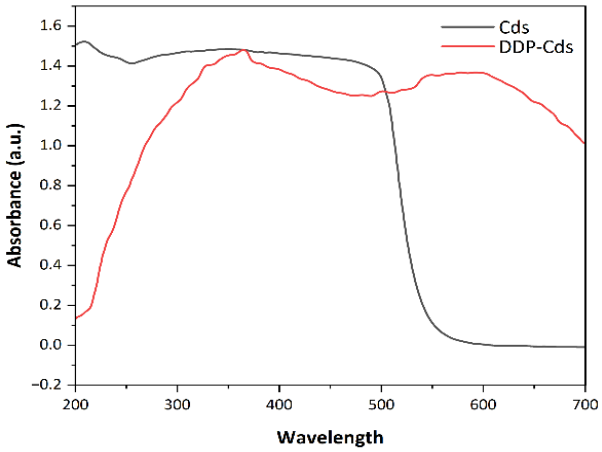

Fig. 4. UV-Vis absorption spectra of CdS and DPP-CdS nanostructures.

3.2. Photovoltaic device performance

To evaluate the impact of DPP-CdS hybrid nanostructures on solar energy conversion, we fabricated bulk heterojunction photovoltaic devices employing three active layers: pure CdS nanoparticles, pure DPP oligomer, and the DPP-CdS hybrid. Devices were constructed in an inverted configuration with the architecture: ITO/PEDOT:PSS/Active Layer/$PC_{71}BM$/Al. This layout was selected for its compatibility with air-stable electrodes and superior charge extraction properties. A schematic diagram of the device structure [18], along with the corresponding energy level alignment of all components, is presented in Figure 5.

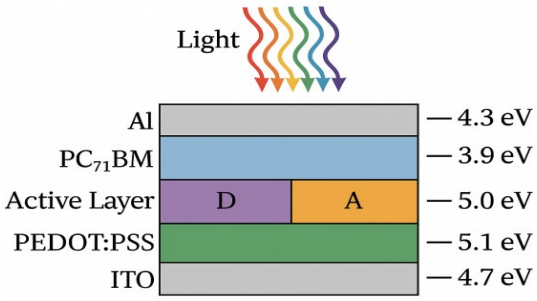

Fig. 5. Schematic illustration of the inverted device structure used in this study: ITO/PEDOT:PSS/Active Layer/$PC_{71}BM$/Al.

The energy level diagram (Figure 6) illustrates that the DPP oligomer possesses a highest HOMO of –5.33 eV and a lowest LUMO of –3.63 eV, while CdS has a conduction band minimum at –4.2 eV and a valence band maximum at –6.5 eV. This configuration facilitates a favorable type-II heterojunction, where photoexcited electrons in DPP can transfer to CdS [19], and holes remain in the DPP phase, promoting effective charge separation and minimizing recombination losses.

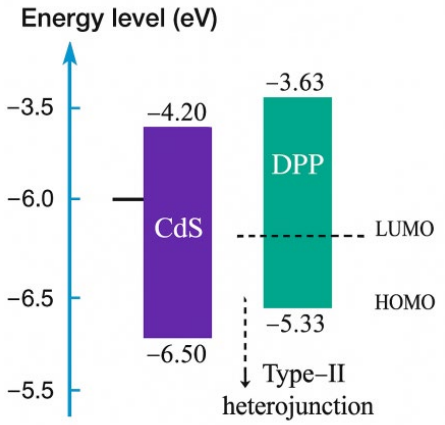

Fig. 6. Energy level diagram showing the relative HOMO/LUMO positions of DPP and conduction/valence bands of CdS, enabling type-II heterojunction alignment and efficient charge separation.

Current density–voltage (J–V) characteristics under AM 1.5G solar illumination (100 mW/cm^2) were recorded to quantify device performance. As shown in Figure 7, the device incorporating the DPP-CdS hybrid exhibited significantly higher photocurrent density and open-circuit voltage compared to devices based solely on CdS or DPP. The DPP-only device yielded a Jsc of 6.1 mA/cm^2, an Voc)of 0.74 V, a FF of 0.58, and a PCE of 2.61%. The CdS-based device showed inferior performance, with a Jsc of 4.2 mA/cm^2 and PCE of 1.35%, attributed to its narrow absorption spectrum and low hole mobility [20]. In contrast, the DPP-CdS hybrid device delivered a Jsc of 11.3 mA/cm², Voc of 0.82 V, FF of 0.64, and a maximum PCE of 5.93%, with an average PCE of 5.77 ± 0.14% across ten independently fabricated devices. The enhanced Jsc is attributed to broadened light absorption and improved charge separation, while the elevated Voc suggests reduced recombination due to optimized interfacial contact [21]. Table 1 summarizes the average photovoltaic parameters of the devices, including standard deviation values to reflect device-to-device reproducibility.

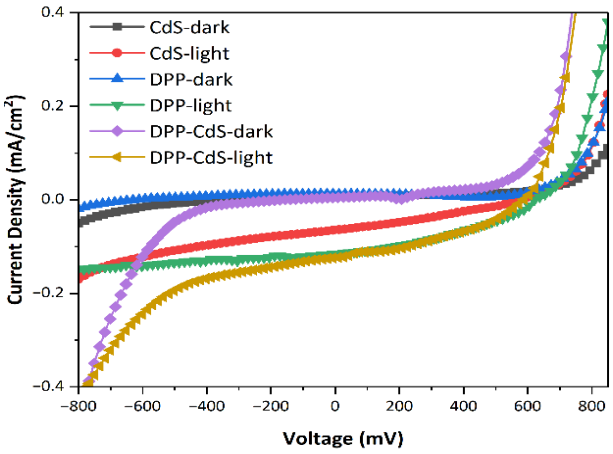

Fig. 7. J–V characteristics of photovoltaic devices based on CdS, DPP, and DPP-CdS hybrid active layers under standard AM 1.5G illumination

.

Table 1. Average photovoltaic performance parameters of devices incorporating different active layers.

Active Layer	**Voc (V)**	**Jsc (mA/cm²)**	**FF**	**PCE (%)**
CdS	0.62	4.2	0.52	1.35
DPP	0.74	6.1	0.58	2.61
DPP-CdS	0.82	11.3	0.64	5.77

To further understand the origin of enhanced photocurrent, external quantum efficiency (EQE) spectra were obtained for all devices and are plotted in Figure 8. The EQE of the CdS device was limited to wavelengths below 520 nm, consistent with its bandgap of ~2.4 eV. The DPP-based device exhibited a broader response extending to 700 nm but with lower magnitude. In comparison, the DPP-CdS hybrid device demonstrated enhanced EQE in both the 400–550 nm and 600–700 nm regions, with a peak quantum efficiency of ~63% at 520 nm. This spectral broadening and intensity increase confirm the complementary absorption and synergistic charge extraction behavior of the hybrid structure [22,23].

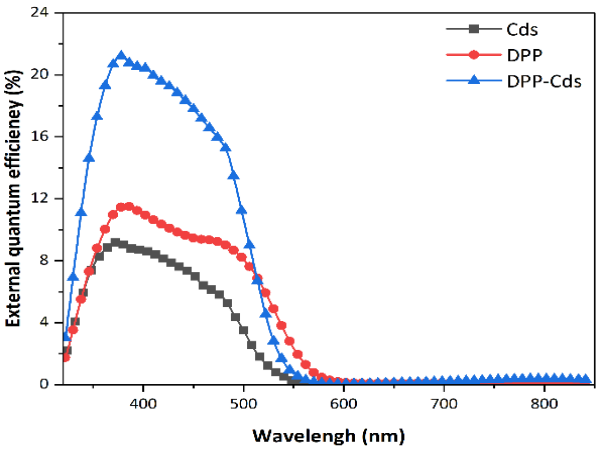

Fig. 8. EQE spectra of devices based on CdS, DPP, and DPP-CdS hybrids.

3.3. Charge transport and recombination dynamics

To further understand the enhanced photovoltaic performance observed in DPP-CdS hybrid devices, a series of electrical and spectroscopic analyses were conducted to investigate charge transport behavior and recombination dynamics. These include electrochemical impedance spectroscopy (EIS), transient photovoltage (TPV) decay analysis, and space-charge limited current (SCLC) modeling. The results provide detailed insights into charge extraction efficiency, internal resistances, trap-induced recombination, and charge carrier mobility in the active layers [24–26].

Electrochemical impedance spectroscopy was performed under dark conditions with a small AC perturbation. The resulting Nyquist plots for the DPP-CdS-based devices are shown in Figure 9. The spectra exhibit a typical semicircular shape, which was fitted using a Randles equivalent circuit. The DPP-CdS device shows a significantly smaller Rct value (~238 Ω) compared to the pure DPP device (~257 Ω) and the CdS-only device (~279 Ω), indicating more efficient charge extraction and reduced interfacial recombination resistance [27,28]. The reduced semicircle diameter in the hybrid device supports the hypothesis of superior carrier transport across the DPP/CdS interface, attributed to the well-aligned energy levels and improved morphology observed in earlier sections [29].

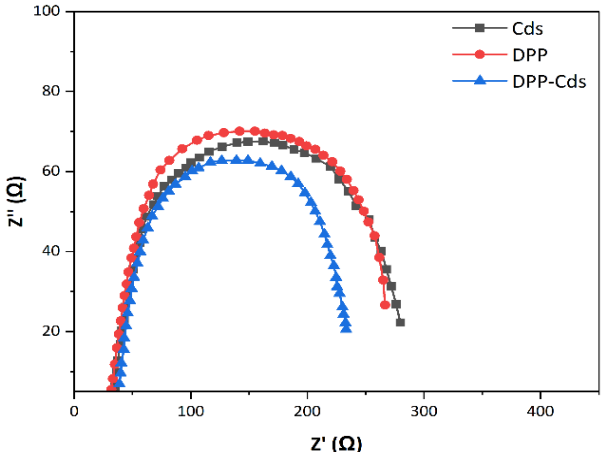

Fig. 9. Nyquist plots of CdS, DPP, and DPP-CdS photovoltaic devices under dark conditions.

To study charge recombination dynamics, TPV measurements were carried out under open-circuit conditions with low-intensity pulsed laser excitation (532 nm). The TPV decay curves are presented in Figure 10, with extracted carrier lifetimes (τ) obtained via exponential fitting. The DPP-CdS hybrid device displayed a much slower voltage decay, corresponding to a lifetime of 6.10 μs, compared to 4.21 μs for DPP and 4.11 μs for CdS. The extended carrier lifetime in the hybrid indicates suppressed recombination losses, further confirming the role of interfacial engineering in stabilizing charge-separated states [30,31].

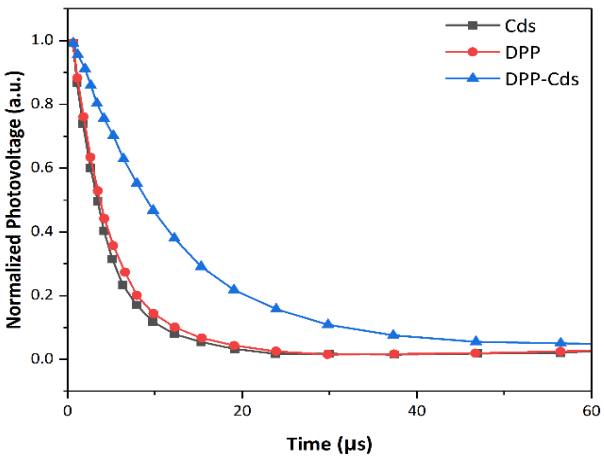

Fig. 10. TPV decay curves of CdS, DPP, and DPP-CdS devices.

4. Conclusion

In conclusion, we successfully designed and synthesized DPP-CdS hybrid nanostructures that exhibit synergistic optoelectronic properties for enhanced photovoltaic applications. Morphological analysis confirmed the homogeneous dispersion of CdS nanoparticles within the DPP matrix, forming interconnected networks favorable for charge transport. Structural and spectroscopic characterization revealed strong interfacial interactions and improved crystallinity, with the hybrid demonstrating a broader absorption spectrum and reduced optical bandgap (~1.92 eV) compared to pristine CdS (~2.38 eV). Photovoltaic devices employing the DPP-CdS active layer in an inverted bulk heterojunction architecture achieved a notable PCE of 5.93%, significantly outperforming devices based on pure DPP (2.61%) and CdS (1.35%). This performance enhancement is attributed to a combination of increased short-circuit current density (11.3 mA/cm^2), elevated open-circuit voltage (0.82 V), and improved fill factor (0.64).

External quantum efficiency measurements revealed peak values up to 63% with broadened spectral response, confirming effective light harvesting and complementary absorption between components. Furthermore, electrochemical impedance spectroscopy and transient photovoltage analysis demonstrated reduced charge transfer resistance (~238 Ω) and prolonged carrier lifetimes (6.10 μs), highlighting improved interfacial contact and suppressed recombination. These findings establish that rational interface engineering between DPP and CdS can yield type-II heterojunctions with superior charge separation and transport characteristics.

The modularity of our synthetic approach, along with its compatibility with scalable solution processing, paves the way for the development of next-generation hybrid solar cells. Future work may explore tuning the DPP chemical structure, optimizing nanoparticle dimensions, or incorporating ternary components to further enhance efficiency and device stability. Overall, this study demonstrates the potential of DPP-CdS hybrid nanostructures as a versatile and effective platform for advancing low-cost, high-performance photovoltaic technologies.

Acknowledgements

This work has been supported by Dongguan Social Development Project General Project (20231800937652), Guangdong University of Science and Technology Research Key Project (GKY-2024KYZDK-5), Guangdong University of Science and Technology Major Research Achievement Cultivation Project (GKY-2022CQPY-2), Guangdong University of Science and Technology Teaching and Technology Innovation Teaching and Learning Enhancement Project (GKJXXZ2023027), Guangdong Province Research Capacity Enhancement Project (2021ZDJS115), Dongguan Science and Technology Bureau Key Project (20231800935832), Dongguan Science and Technology Special Envoy Project (20231800500582).

References

[1] K. Ahmad, H. Kim, Inorganic Chemistry Communications 165, 112546 (2024); https://doi.org/10.1016/j.inoche.2024.112546

[2] T. Amrillah, Solar Energy 263, 111982 (2023); https://doi.org/10.1016/j.solener.2023.111982

[3] S. Barthwal, S. Singh, A. K. Chauhan, R. Karuppannan, ACS Sustainable Chemistry & Engineering 12, 947 (2024); https://doi.org/10.1021/acssuschemeng.3c06210

[4] M. G. Buonomenna, Symmetry 15, 1718 (2023); https://doi.org/10.3390/sym15091718

[5] F. Butrichi, V. Trifiletti, G. Tseberlidis, B. E. G. Colombo, F. Taglietti, M. Rancan, L. Armelao, S. Binetti, Solar Energy Materials and Solar Cells 272, 112924 (2024); https://doi.org/10.1016/j.solmat.2024.112924

[6] M. Chen, J. Ma, C. Chen, J. Ding, Y. Liu, H. He, Q. Liu, G. Hu, Y. Wu, X. Liu, Chemical Engineering Journal 498, 155302 (2024); https://doi.org/10.1016/j.cej.2024.155302

[7] M. Farji, Brazilian Journal of Physics 51, 1916 (2021); https://doi.org/10.1007/s13538-021-00981-w

[8] I. M. Dharmadasa, A. E. Alam, A. A. Ojo, O. K. Echendu, Journal of Materials Science: Materials in Electronics 30, 20330 (2019); https://doi.org/10.1007/s10854-019-02422-6

[9] L. Hafaifa, M. Maache, Z. Allam, A. Zebeir, Results in Optics 14, 100596 (2024); https://doi.org/10.1016/j.rio.2023.100596

[10] R. Get, Sk. M. Islam, S. Singh, P. Mahala, Optik 266, 169560 (2022); https://doi.org/10.1016/j.ijleo.2022.169560

[11] N. Kant, P. Singh, Materials Today: Proceedings 56, 3460 (2022); https://doi.org/10.1016/j.matpr.2021.11.116

[12] S. Khan, M. Z. Iqbal, A. Zakir, A. Khizar, Z. Liu, M. H. Sayyad, S. M. Wabaidur, N. Badi, Solar Energy 274, 112593 (2024); https://doi.org/10.1016/j.solener.2024.112593

[13] R. Malani, T. Pansuriya, V. Kheraj, Optical Materials 133, 112910 (2022); https://doi.org/10.1016/j.optmat.2022.112910

[14] D. Lilhare, A. Khare, Opto-Electronics Review Vol. 28, No. 1, (2020).

[15] Mamta, K. K. Maurya, V. N. Singh, Coatings 12, 405 (2022); https://doi.org/10.3390/coatings12030405

[16] A. S. Najm, P. Chelvanathan, S. K. Tiong, M. T. Ferdaous, S. A. Shahahmadi, Y. Yusoff, K. Sopian, N. Amin, Coatings 11, 52 (2021); https://doi.org/10.3390/coatings11010052

[17] D. B. Mitzi, Y. Kim, Faraday Discussions 239, 9 (2022); https://doi.org/10.1039/D2FD00132B

[18] C. Nicolaou, A. Zacharia, A. Delimitis, G. Itskos, J. Giapintzakis, Applied Surface Science 511, 145547 (2020); https://doi.org/10.1016/j.apsusc.2020.145547

[19] J. Pastuszak, P. Węgierek, Materials 15, 5542 (2022); https://doi.org/10.3390/ma15165542

[20] D. Payno, Y. Sánchez, O. Blázquez, S. Giraldo, M. Salado, S. Kazim, E. Saucedo, S. Ahmad, Journal of Materials Chemistry C 8, 12533 (2020); https://doi.org/10.1039/D0TC02666B

[21] T. Raadik, N. Spalatu, J. Krustok, R. Josepson, M. Grossberg, Thin Solid Films 743, 139069 (2022); https://doi.org/10.1016/j.tsf.2021.139069

[22] M. A. Rahman, SN Applied Sciences 3, 253 (2021); https://doi.org/10.1007/s42452-021-04267-3

[23] Md. F. Rahman, Md. M. Tasdid, M. M. Fadhali, M. Sharma, M. Akermi, Photonics and Nanostructures - Fundamentals and Applications 64, 101371 (2025); https://doi.org/10.1016/j.photonics.2025.101371

[24] Md. A. Razzaque, A. T. Abir, S. S. Nushin, J. Hossain, Next Research 2, 100135 (2025); https://doi.org/10.1016/j.nexres.2025.100135

[25] D. Rovira, E. Ros, T. Tom, M. Jiménez, J. Miguel Asensi, C. Voz, J. López-Vidrier, J. Puigdollers, J. Bertomeu, E. Saucedo, International Journal of Molecular Sciences 24, 3088 (2023); https://doi.org/10.3390/ijms24043088

[26] U. Saha, A. Biswas, Md. K. Alam, Solar Energy 221, 314 (2021); https://doi.org/10.1016/j.solener.2021.04.043

[27] S. Sajjad, M. H. Sayyad, N. Khan, T. Manzoor, N. Nasr, R. A. Toor, S. A. A. Shah, Z. Guo, Materials Science and Engineering: B 273, 115437 (2021); https://doi.org/10.1016/j.mseb.2021.115437

[28] B. Saparov, Chemical Reviews (2022).

[29] Md. S. Shah, Md. K. Hasan, S. C. Barman, J. A. Bhuiyan, H. Mamur, M. R. A. Bhuiyan, Next Research 2, 100143 (2025); https://doi.org/10.1016/j.nexres.2025.100143

[30] T. D. Siegler, T. M. Shimpi, W. S. Sampath, B. A. Korgel, Chemical Engineering Science 199, 388 (2019); https://doi.org/10.1016/j.ces.2019.01.003

[31] G. Tseberlidis, C. Gobbo, V. Trifiletti, V. Di Palma, S. Binetti, Sustainable Materials and Technologies 41, e01003 (2024); https://doi.org/10.1016/j.susmat.2024.e01003